J. CHEM. SOC. FARADAY TRANS., 1994, 90(18), 2671–2675

Effects encountered in EPR Spectroscopy and Imaging at Small Magnetic Fields

Duncan G. Gillies, Leslie H. Sutcliffe and Mark R. Symms†
Chemistry Department, University of Surrey, Guildford, Surrey, UK GU2 5XH

In vivo EPR studies of biological systems and other 'wet' systems are often performed at radiofrequencies (low static magnetic fields) in order to minimize conductive losses incurred with relatively large samples. Here, attention is drawn to several consequences which can arise from carrying out EPR spectroscopy and imaging (EMRI) at low fields. The first causes a distortion of the gradient when the applied gradient is not a small fraction of the external magnetic field. These 'concomitant gradients' could pose problems if high-resolution imaging experiments are attempted. Other phenomena stem from the Breit–Rabi effect which causes spectral distortions and has implications for data acquisition and image processing. A third effect is the near removal of g factor anisotropy resulting from using low magnetic fields. Thus the powder spectrum for a typical aminoxyl radical is completely different from that observed at X-band: this has consequences for both imaging and for the measurement of rotational diffusion constants. It is shown that there are disadvantages in using ^{15}N- labelled spin probes/labels for EPR measurements at radiofrequencies.

As in NMR spectroscopy, sensitivity increases with frequency for EPR spectroscopy. At the typical microwave frequency of 9 GHz (X-band), the effective sample volume is about 0.3 cm^3, but conductive losses encountered with 'wet' samples can reduce this volume to about 0.03 cm^3. Thus, in order to study large 'lossy' samples by EPR spectroscopy it is necessary to use irradiating frequencies $\lesssim 1$ GHz and, for many purposes, frequencies of about 200 MHz are more appropriate.[1] The typical nitrogen hyperfine interaction for an aminoxyl spin probe is *ca.* 40 MHz, which is not small compared with the irradiating frequency at these low frequencies (fields). In this paper, we present three consequences arising from carrying out EPR experiments at radiofrequencies: (i) concomitant gradient effects in imaging, (ii) Breit–Rabi effects in spectroscopy and imaging, (iii) the effect of the near elimination of g anisotropy on 'powder' spectra and motional studies.

Concomitant Gradient Effects in Radiofrequency (RF) Imaging

Electron magnetic resonance imaging (EMRI) has proved to be a very useful technique for studying the spatial distribution of free radicals in a sample.[1] The basic principle behind the method is very similar to that of the ubiquitous NMR equivalent, namely MRI, but continuous wave (CW) rather than pulse techniques are almost always used owing to the short electron T_2. A magnetic resonance line is broadened inhomogeneously by applying a linear magnetic field gradient in order to 'frequency-encode' (or more exactly, 'gradient-encode') the spins in space. Major differences are (i) the applied magnetic field is only 7 mT for EMRI at 200 MHz, (ii) the short electron spin–spin relaxation time and relatively large electron magnetogyric ratio make pulsed EMRI very difficult to implement, (iii) the large linewidth requires magnetic field gradients as large as 1000 mT m^{-1}. The maximum gradient applied in practice is quite often determined by (*a*) the power supply available, (*b*) gradient coil heating problems, (*c*) the acceptable loss of signal : noise ratio: RF EMRI systems suffer particularly from low signal : noise ratios. However, as larger field gradients are used in the quest for increased resolution, low-field EMRI may start to violate a restriction noted in MRI, namely that the gradient field must be a small perturbation of the main magnetic field.[2] Interestingly, an alternative EMRI technique has been proposed that does not require field gradients.[3]

† This paper was presented at the 27th International ESR conference at the University of Wales, Cardiff, 21st–25th March, 1994.

Gradient Requirements for NMR and EPR

As is well known, to obtain a resolution of δx for a sample of linewidth proportional to $1/T_2$, the minimum gradient needed, G, is determined by the imaging version of the Rayleigh criterion:[2]

$$G > 1/(T_2\gamma\delta x) \tag{1}$$

where γ is defined in a manner compatible with NMR, that is, $\omega = \gamma B$. Thus for NMR and EPR experiments of the same resolution:

$$[GT_2\gamma_e\delta x]_{EPR} = [GT_2\gamma_n\delta x]_{NMR} \tag{2}$$

Hence, for T_2 (NMR) = 0.1 s and T_2 (EPR) = 350 ns:

$$G_{EPR} = 434G_{NMR} \tag{3}$$

Concomitant Gradients

Maxwell's equations for a magnetic field in free space forbid the existence of a single pure linear magnetic field gradient. However, from the theoretical basis of MRI[2] it can be seen that the application of a gradient field is most accurately described as a tensor, and only for large static main fields and small gradients can the latter be expressed as a vector perturbation. For small static fields, higher-order terms will appear giving concomitant gradients that can cause various image distortions.[4] The latter are observed in MRI in the phase-encoding direction in several experiments, as this direction usually has a much smaller frequency per pixel than the frequency-encoding direction and is therefore more susceptible to distortion from flow artifacts, chemical shift or concomitant gradients. However, apart from one interesting exception,[9] CW imaging relies exclusively upon frequency-encoding gradients. Nevertheless, EMRI is potentially more vulnerable than MRI to concomitant effects, so we will now use the analysis of Norris and Hutchison[4] to predict the nature and extent of the effects in frequency encoding.

If we have a static field along the z axis:

$$\boldsymbol{B}_0 = B_0\boldsymbol{k} \tag{4}$$

and a gradient field:

$$\boldsymbol{B}(x) = xG\boldsymbol{k} \tag{5}$$

then in order to satisfy Maxwell's equation for free space:

$$\text{curl } \boldsymbol{B} = 0 \tag{6}$$

an extra (concomitant) gradient term is created such that:

$$\boldsymbol{B}(x, z) = xG\boldsymbol{k} + zG\boldsymbol{i} \tag{7}$$

The resulting applied field is:

$$[B(x, z)]^2 = (B_0 + xG)^2 + (zG)^2 \tag{8}$$

Expanding this to second order gives:

$$B(x, z) = B_0 + xG + (zG)^2/2B_0 \tag{9}$$

In CW EMRI, a linear magnetic field gradient $G = dB_z/dx$ is applied to the sample then the static field is swept slowly through resonance tracing a broadened spectrum. An advantageous feature in certain applications is that the sample is swept from one side of the gradient-labelled space to the other. Thus for a given value of sweep, B_s, the signal arises from the shaded region shown in Fig. 1: there is a yz plane of spins proportional in width to $1/T_2$, such that:

$$B_0 + Gl + B_s = \omega/\gamma_e \tag{10}$$

where ω is the angular resonant frequency and Gl is defined in Fig. 1. The gradient-broadened spectrum can be considered to be the projection of the spin density of the sample taken in the direction of the applied linear gradient. A typical projection-reconstruction imaging experiment would continue by incrementing the direction of the gradient through all possible angles in three-dimensional (3D) space.[5] The concomitant effect causes the volume of spins now contributing to the signal at a particular value of the sweep field to be curved. This curvature is the first consequence of the concomitant gradient. Depending on the magnitudes of the main fields and the gradients used, it could cause problems when using frequency-encoding gradients in EMRI; it could also cause extra dephasing of the signal during the selection procedure in a pulse FT EMRI experiment.

Size of Concomitant Distortions

At present, the signal : noise ratios of most RF EPR spectrometers are too low to allow images to be taken with high enough resolution for the concomitant effect to be noticeable. However, the size of the effect can be estimated using a typical set of parameters, namely: $T_2 = 350$ ns (a typical value for an *in vivo* aminoxyl radical); $\delta x = 5$ mm (a typical pixel size); $B_0 = 7$ mT (corresponding to a RF of 200 MHz); $r = 0.1$ m (sample radius, 40 pixels per projection permitted). From eqn. (1), $G \approx 3$ mT m^{-1}, thus each pixel has a bandwidth of $1/T_2 = 2.8$ MHz. The concomitant distortion, $E = \gamma(Gr)^2/2B_0$, is 1.3 MHz or about half a pixel at worst. A more ambitious set of parameters would give worse distortions.

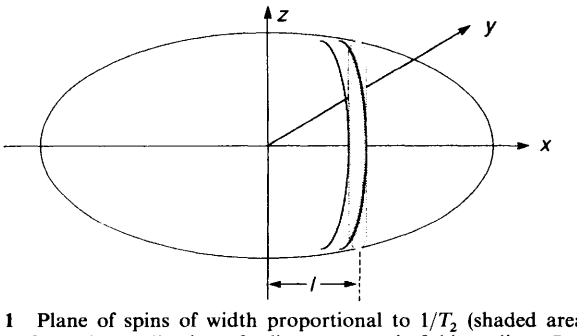

Fig. 1 Plane of spins of width proportional to $1/T_2$ (shaded area) arising from the application of a linear magnetic field gradient $G = dB_z/dx$ in the CW EMRI experiment. The adjacent curved area is the region actually sampled due to the concomitant gradient effect.

The relative distortion, d, or distortion per pixel bandwidth is given by:

$$d = ET_2 = T_2\gamma(Gr)^2/2B_0 \tag{11}$$

Thus it may be seen that the concomitant distortion is made worse by use of (*a*) a low-field spectrometer, (*b*) large samples, (*c*) spin probes with large linewidths.

Effect of Field Sweep

The considerations given apply most accurately to a frequency-swept CW experiment. In a field-swept experiment, the full extent of the sweep field can no longer be regarded as a small perturbation of the static field since the nitrogen hyperfine splitting in an aminoxyl radical is *ca.* 1.5 mT (≡40 MHz). In this situation, the concomitant distortion is given by:

$$B(x, z) = B_0 + [(zG)^2/2(B_0 + B_s)] \tag{12}$$

It can be seen that the concomitant curvature will be more pronounced at the low-field end of the sweep. For example, using a total sweep of 5 mT, centred on 7 mT (≡200 MHz), eqn. (12) gives a concomitant distortion that is about twice as bad at the low-field as at the high-field end of the sweep. Of course, the effect will be absent for some of the recently reported single-line spin probes.[6,7]

Comparison of Concomitant Effects in EMRI and MRI

From eqn. (11) and the optimum gradient strength $G = 1/(T_2\gamma\delta x)$ and $r = n\delta x$ (where n is the number of pixels in a projection) we obtain:

$$d = n^2/(2\omega T_2) \tag{14}$$

In order to compare EMRI with MRI, the ideal approach would be to take two systems of similar signal : noise ratios. However, this would require an extensive analytical comparison of CW EPR with FT NMR which is beyond the scope of this paper. Instead, we shall compare the two magnetic resonances at (*a*) equal main field and (*b*) equal Larmor frequency.

(*a*) Equal main field

$$d_{NMR} = d_{EPR}\,\gamma_e\,T_2(\text{EPR})/T_2(\text{NMR})\gamma_n \tag{15}$$

thus

$$d_{NMR} = d_{EPR}/434$$

(*b*) Equal Larmor frequency

$$d_{NMR} = d_{EPR}\,T_2(\text{EPR})/T_2(\text{NMR}) \tag{16}$$

thus

$$d_{NMR} = d_{EPR}/285714$$

The second case probably provides the better comparison between the two modalities. The equations suggest that concomitant gradients may have a part to play in limiting the ultimate resolution achievable in low-field EMRI.

Concomitant Effects in Overhauser Imaging

Overhauser imaging (variously called DNP imaging[8] or PEDRI[9]) uses EPR to enhance the NMR (usually proton) signal. Apart from the opportunities afforded by cycling the main field, these techniques are similarly limited in sample size by conductive losses. Thus it is to be expected that conco-

mitant gradient effects will occur. The original paper by Norris and Hutchison[4] contains results obtained with a low-field MRI system which illustrate some of the phase-encoded distortions that are likely to be encountered in Overhauser imaging.

Breit–Rabi Effects

Second-order effects are encountered in EPR spectra when hyperfine interactions represent a significant fraction of the main magnetic field, B_0. For solution spectra at X-band frequencies (7.8–12.4 GHz), when there are two or more equivalent magnetic nuclei present, extra lines may be observed (owing to the lifting of degeneracy) if the isotropic hyperfine interaction, a, is larger than *ca.* 4 mT. Even when only one magnetic nucleus is present with $I > 1/2$, there are inequalities in the observed splittings (separations increasing with magnetic field); hence the magnitude of the hyperfine interaction cannot be read directly from the spectra. In addition, the centre of the spectrum does not necessarily correspond to the g factor. However, even for the smaller a values, *ca.* 1.5 mT, typical of the aminoxyl nitrogen isotropic hyperfine interaction, precision work at X-band frequencies requires corrections to be made for both a (*ca.* 0.4%) and the g factor.

As noted above, in RF EPR spectroscopy and imaging the applied magnetic field is only of the order of 10 mT and this can lead to very large second-order effects for aminoxyls: it is the ratio of the applied magnetic field to the hyperfine interaction which produces the effects. The mathematics were worked out by Breit and Rabi[10,11] from Stern–Gerlach experiments, long before magnetic resonance was discovered. When the high-field approximation (the Paschen–Back effect in atomic spectra) is not valid, the complete decoupling of the electron and nuclear spins, S and I, cannot be assumed and the quantum numbers F and M_F are now 'good' quantum numbers.[12] For $I = 1$, F has values of 1/2 and 3/2, thus when B_0/a is relatively small, there are the energy states $E(F, M_F)$, which are explicitly:

$$E(+1/2, +1/2);\ E(+1/2, -1/2);\ E(+3/2, +3/2);$$

$$E(+3/2, +1/2);\ E(+3/2, -1/2);\ E(+3/2, -3/2).$$

Since the selection rules are $\Delta M_F = 0$ for $F = 0$ states and $\Delta M_F = 0, \pm 1$ for other F states, there are a total of six allowed transitions[11] as zero field is approached (see Fig. 2). Four of the six transitions are of the π type ($\Delta M_F = \pm 1$), being polarized in the x or y directions, while two of the transitions ($\Delta M_F = 0$) are of the σ type, being polarized in the z direction. This situation is to be compared with the three transitions observed at high fields for $I = 1$. Experiments were carried out by Decorps and Fric[13] who obtained EPR spectra from aqueous solutions of Fremy's salt (potassium peroxylamine disulfonate) at 80 and 210 MHz. At the higher frequency, the applied magnetic field is sufficiently large to almost exclude the σ transitions, but at 80 MHz the randomly oriented permanent magnetic field from the ^{14}N nucleus is competing strongly with the main magnetic field in the z direction, thus both σ and π transitions were observed. Recently, Guiberteau and Grucker[14] have demonstrated that dynamic nuclear polarization with σ-transition EPR irradiation is allowed at low magnetic fields and that with fields lower than 1.7 mT, saturation of σ transitions is more efficient than that for saturation of the π transitions. Decorps and Fric[13] also recorded the EPR spectrum of DPPH (α,α′-diphenyl-β-picrylhydrazyl) in benzene and found that the spectrum at 40 MHz is compressed compared with spectra obtained at higher frequencies, that is, it is part way to becoming a single line. Note that at zero field, linewidths are narrow (*ca.* 0.5 MHz) and only one line is observed having an energy of $a(I + 1/2)$: a definitive review of zero-field EPR spectroscopy has been published by Bramley and Strach.[15] If third-order corrections are neglected, the hyperfine coupling constant can be determined for integral nuclear spins from the separation ($=2Ia$) of the extreme hyperfine lines, and for half-integral spins from the separation ($=a$) of the $M_I = \pm 1/2$ lines. An excellent paper by Boate *et al.*[12] describes the effect of very large isotropic hyperfine interactions (up to *ca.* 1900 mT) at X-band frequencies, which cause the recorded EPR spectra to bear no resemblance to the hyperfine patterns predicted by first-order theory. When a very large hyperfine interaction is present, only one EPR line is accessible corresponding to $M_I = -I$ (for positive a values): other mixed transitions may appear having intensities comparable to the EPR lines. They showed that the remaining EPR lines are observable only at microwave frequencies in excess of $(I + 1/2)g\beta a$.

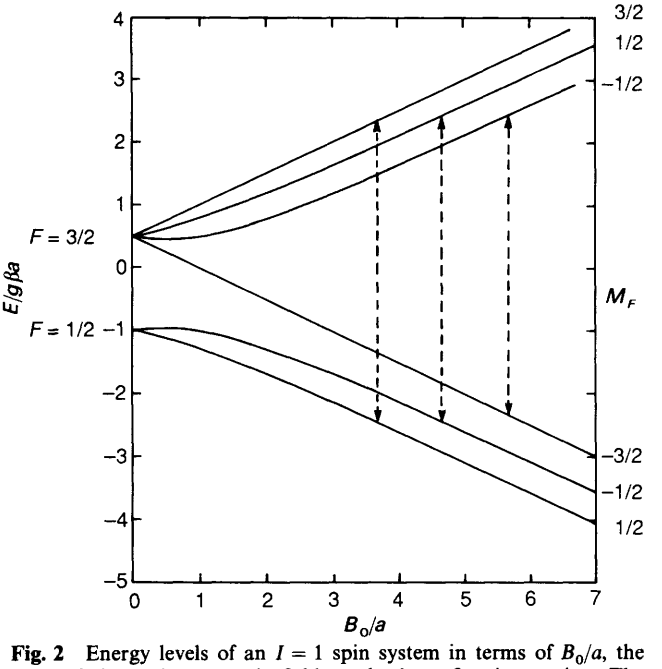

Fig. 2 Energy levels of an $I = 1$ spin system in terms of B_0/a, the ratio of the main magnetic field to the hyperfine interaction. The vertical lines represent the transitions for $a = 1.5$ mT and $B_0 = 7$ mT.

Currently, there is an interest in low-field EPR spectroscopy because of the wealth of biological problems that can be tackled with 'lossy' samples. Some published RF spectra of aqueous aminoxyl solutions show uneven line spacings, but none of the authors concerned have drawn attention to this fact: a selection of such data is shown in Table 1. The ratios of the splittings observed experimentally correspond to those predicted by diagonalization of the energy matrix. Thus these

Table 1 Splittings observed for aminoxyl radicals at low fields

radical	spectrometer frequency /MHz	splitting/mT		ratio of splittings		ref.
		+1, 0	0, −1	obs.[a]	calc.[b]	
CTPO	790	1.615	1.692	0.954	0.951	16
4-oxo-TEMPO	300	1.615	1.800	0.897	0.870	17
Fremy's salt	280	1.247	1.443	0.864	0.861	18
Fremy's salt	210	1.241	1.459	0.851	0.821	13
tert-Bu_2NO	200	1.558	2.013	0.774	0.795	19
Fremy's salt	80	0.983	1.761	0.558	0.593	13

[a] Measured from published spectra. [b] Calculated using the program QPOWA.

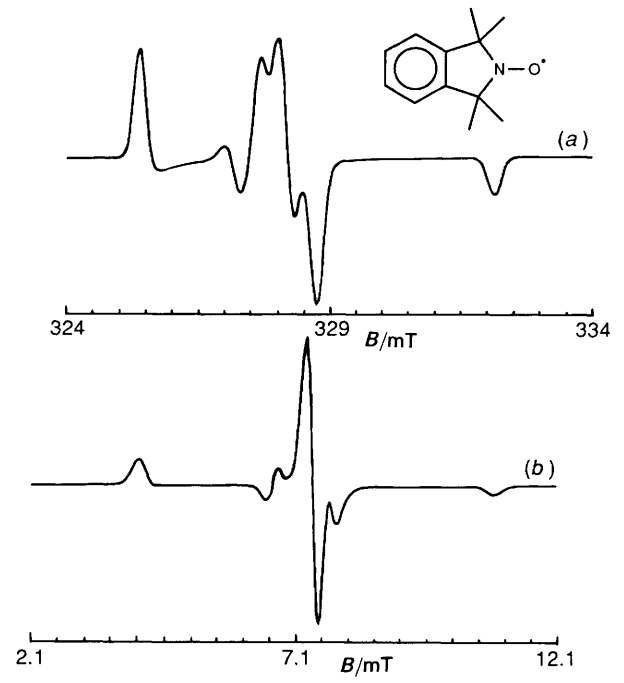

Fig. 3 9.2 GHz (*a*) and 200 MHz (*b*) (computed) rigid limit spectra of the 1,1,3,3-tetra[$^2H_3$]methylisoindolin-2-yloxyl radical

ratios can be used to check the linearity of the field sweep of low-field EPR spectrometers.

Note, for the aminoxyl radical data given in Table 1, for frequencies less than *ca.* 100 MHz, that the centre line becomes relatively less intense than the outer lines, and the low-field line is more intense than that at high fields. Above 200 MHz, *a* may be determined reliably as half the separation of the outer lines.

Implications for Low-field EMRI

The intrinsic dependence of the line position on the externally applied magnetic field caused by the Breit–Rabi effect suggests that a large imaging gradient might apply additional

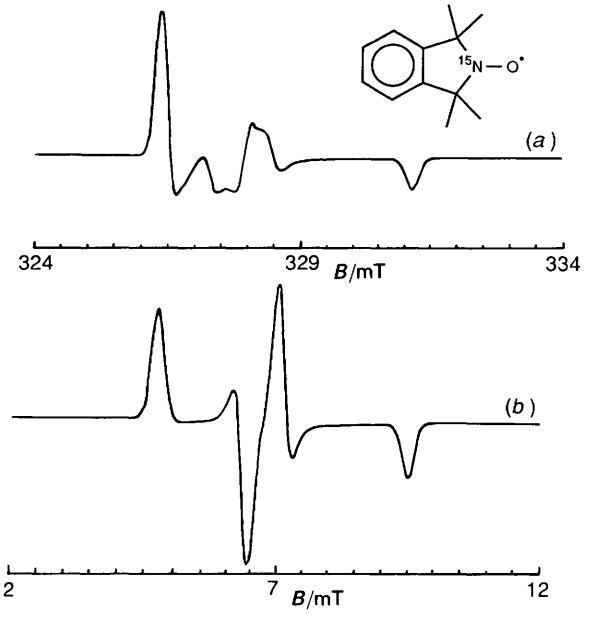

Fig. 4 9.2 GHz (*a*) and 200 MHz (*b*) (computed) rigid limit spectra of the [^{15}N]-1,1,3,3-tetra[$^2H_3$]methylisoindolin-2-yloxyl radical

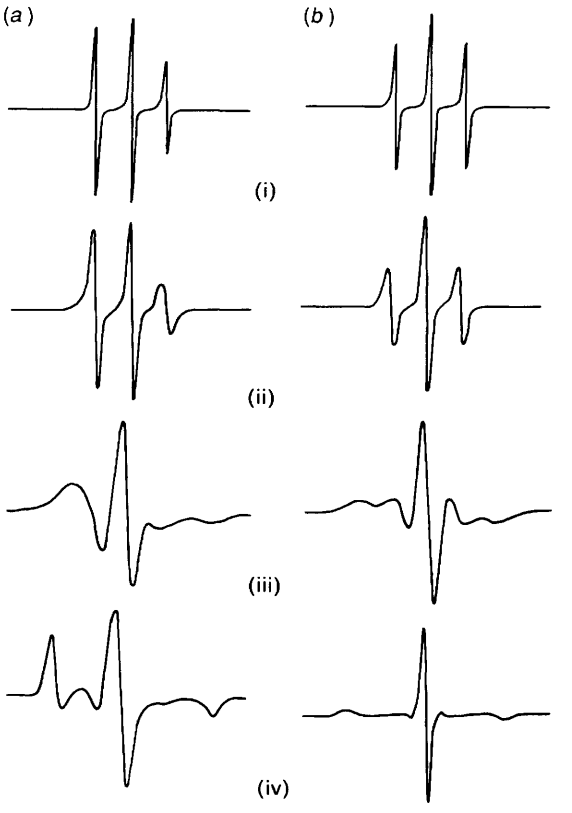

Fig. 5 Computed 9.2 GHz (*a*) and 200 MHz (*b*) spectra of 1,1,3,3-tetra[$^2H_3$]methylisoindolin-2-yloxyl radical for rotational diffusion constants of (i) 10^9 s^{-1}, (ii) 2×10^8 s^{-1}, (iii) 3×10^7 s^{-1}, (iv) 5×10^6 s^{-1}. A linewidth of 0.04 mT was used in the calculations. The field sweep is 10 mT. Note that the total intensities of the spectra are not to scale.

undesirable position-dependent dispersion to the broadened spectrum. In fact, it seems that for the most common EMRI experiment, namely field-swept CW EMRI, each part of the resonance is brought on to resonance at a constant frequency by the field sweep, hence no distortion is introduced. For Fourier transform or (as yet, hypothetical) frequency-swept EMRI, the Breit–Rabi effect will cause the frequency of spins to be non-linearly related to their position, thus producing image distortions. In principle, as the non-linearity is known, it should be possible to apply a post-processing correction during image reconstruction at the expense of incurring variable resolution across the image.

Near Removal of *g* Factor Anisotropy

The nature of a powder spectrum is determined by the anisotropy of the *g* factors and of the hyperfine interactions. The presence of these anisotropies is utilised in spin probe/label experiments that are normally carried out at X-band frequencies. However, EPR spectra obtained at radiofrequencies can have a completely different appearance since the *g* factor anisotropy essentially disappears (the hyperfine anisotropy remains), the consequences of which are discussed below.

Imaging

A powder X-band spectrum of a typical aminoxyl radical (1,1,3,3-tetra[$^2H_3$]methylisoindolin-2-yloxyl,[20] [$^2H_{12}$]TMIO) is shown in Fig. 3(*a*). Owing to its complexity and large linewidths this spectrum would not be suitable for solid-state imaging. However, using the simulation program QPOWA

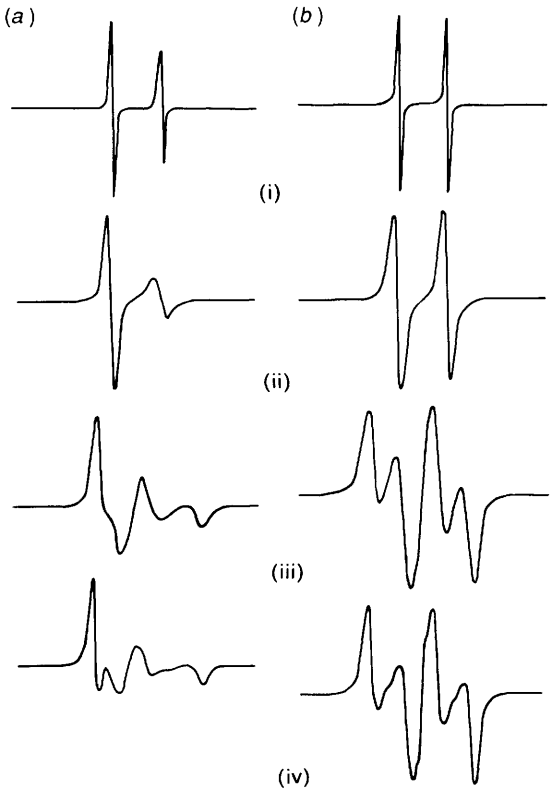

Fig. 6 Computed 9.2 GHz (*a*) and 200 MHz (*b*) spectra of [^{15}N]-1,1,3,3-tetra[$^{2}H_3$]methylisoindolin-2-yloxyl radical for rotational diffusion constants of (i) 10^9 s^{-1}, (ii) 10^8 s^{-1}, (iii) 10^7 s^{-1}, (iv) 5×10^6 s^{-1}. A linewidth of 0.04 mT was used in the calculations. The field sweep is 10 mT. Note that the total intensities of the spectra are not to scale.

the RF EPR spectrum of the same radical [see Fig. 3(*b*)] is essentially a single narrow line and thus has imaging potential. By contrast, it may be seen from Fig. 4 that the reverse is true for the QPOWA-simulated spectrum of the ^{15}N-substituted radical. The sharpness of the rigid limit central line of the ^{14}N-containing radical may be seen by comparing the fast and slow rotational spectra shown in Fig. 5.

Rotational Diffusion

Using the computer program devised by Schneider and Freed,[21] we have simulated sets of spectra for [$^{2}H_{12}$]TMIO and its ^{15}N analogue for a series of rotational diffusion constants. This has been done for spectra at X-band and at 200 MHz. Since the program requires the high-field approximation to hold we have obtained the latter by converting the g factors to their equivalents at X-band. Thus, the actual values[20] of $g_{xx} = 2.00820$, $g_{yy} = 2.00523$ and $g_{zz} = 2.00147$ become 2.00504, 2.00498 and 2.00490, respectively: the corresponding hyperfine interactions remain unchanged at 3.382, 0.439 and 0.500 mT for ^{14}N. Fig. 5 shows the results obtained for [$^{2}H_{12}$]TMIO at 9.2 GHz and at 200 MHz. The former show the familiar pattern as the rotational diffusion constant is decreased: in the 'fast' regime this constant can be calculated in the usual way[22] from the asymmetric line broading. In the slow region which occurs (for example) in solid polymers, motion is measured from the extrema of the powder-like spectra.[23] The spectra simulated for the ^{15}N- labelled radical are shown in Fig. 6. Again, rotational diffusion constants could be derived for the 'fast' region from the asymmetric line broadening of the X-band spectra. For the RF spectra, band-shape analysis would have to be employed to obtain the constants for the fast motional regime.

Note that because the high-field approximation has been used to calculate the RF spectra, they do not show the Breit–Rabi effect as they should.

To summarise this section, ^{15}N-labelling is advantageous for Overhauser enhancement at radiofrequencies, but it is disadvantageous for both radiofrequency spectroscopy and imaging.

M.R.S. is indebted to SERC for financial support. We also wish to thank Dr. Gorazd Planinsic and Dr. K. F. Preston for helpful discussions, Profs. R. L. Belford and M. J. Nilges for allowing us to use their QPOWA computer program, and Dr. S. A. Fairhurst for her assistance.

References

1 G. R. Eaton, S. S. Eaton and K. Ohno, *EPR Imaging and In Vivo EPR*, CRC Press, Boca Raton, Florida, 1991.
2 P. Mansfield and P. G. Morris, *NMR Imaging in Medicine*, Academic Press, New York, 1982.
3 E. Szczepaniak and J. P. Hornak, *J. Magn. Reson.*, 1993, **A104**, 315.
4 D. G. Norris and J. M. S. Hutchison, *Magn. Reson. Imaging*, 1990, **8**, 33.
5 R. K. Woods, G. G. Bacic, P. C. Lauterbur and H. M. Swartz, *J. Magn. Reson.*, 1989, **84**, 247.
6 P. Turek, J-J. Andre, M. Moussavi and G. Fillion, *Mol. Cryst. Liq. Cryst.*, 1989, **176**, 535.
7 G. Bacic, K. J. liu, J. A. O'Hara, R. D. Harris, K. Szybinski, F. Goda and H. M. Swartz, *Magn. Reson. Med.*, 1993, **30**, 568.
8 D. Grucker, *Magn. Reson. Med.*, 1990, **14**, 140.
9 D. J. Lurie, D. M. Bussell, L. H. Bell and J. R. Mallard, *J. Magn. Reson.*, 1988, **76**, 366.
10 G. Breit and I. I. Rabi, *Phys. Rev.*, 1931, **8**, 2082L.
11 J. E. Nafe and E. B. Nelson, *Phys. Rev.*, 1948, **73**, 718.
12 A. R. Boate, J. R. Morton and K. F. Preston, *J. Magn. Reson.*, 1976, **24**, 259.
13 M. Decorps and C. Fric, *J. Phys. E: Sci. Instrum.*, 1972, **5**, 337.
14 T. Guiberteau and D. Grucker, *J. Magn. Reson.*, 1993, **A105**, 98.
15 R. Bramley and S. J. Strach, *Chem. Rev.*, 1983, **83**, 49.
16 S. Ishida, H. Kumashiro, N. Tsuchihashi, T. Ogata, M. Ono, H. Kamada and E. Yoshida, *Phys. Med. Biol.*, 1989, **34**, 1317.
17 J. A. Brivati, A. D. Stevens and M. C. R. Symons, *J. Magn. Reson.*, 1991, **92**, 480.
18 M. Alecci, S. D. Penn, A. Sotgiu, L. Testa and I. Vannucci, *Rev. Sci. Instrum.*, 1992, **63**, 4263.
19 J. P. Hornak, M. Spacher and R. G. Bryant, *Meas. Sci. Technol.*, 1991, **2**, 520.
20 R. Bolton, D. G. Gillies, L. H. Sutcliffe and X. Wu, *J. Chem. Soc., Perkin Trans. 2*, 1993, 2049.
21 D. J. Schneider and J. H. Freed, in *Biological Magnetic Resonance*, ed. L. J. Berliner, Plenum, New York, 1989, vol. 8, p. 1.
22 P. L. Nordio, in *Spin Labeling, Theory and Applications*, ed. L. J. Berliner, Academic Press, New York, 1976.
23 P. Törmälä, G. Weber and J. J. Lindberg, in *Molecular Motion in Polymers by ESR*, ed. R. F. Boyer and S. E. Keinath, Harwood, New York, 1980.

Paper 4/02219J; *Received* 14*th April*, 1994